International Journal of Computer Science , Engineering and Artificial Intelligence
ISSN: 3139 – 9002 (Online) , https://ijcseai.com/
Regular Issue, Vol. 2, Issue. 4 (October – December) , 2025 , Pages: 1 - 6
Received: 27 March 2024 ; *Accepted:* 02 September 2025 ; *Published:* 05 October 2025
https://doi.org/10.63328/IJCSEAI-V2RI4P1
https://www.youtube.com/watch?v=Or7FvOcW6gY
https://archive.org/details/jsp-ijcseai-v2ri4p1
Original Paper : Action Research – Experimental Research Paper

Graph Neural Networks with Riemannian Brain Connectivity Analysis for EEG-Based Neurological Classification

Sivaram Murugan

Department of Computer Engineering, Sivas University of Science and Technology, Sivas, Turkey - 58000

* *Corresponding Author : Sivaram Murugan ; sivaram.murugan@sivas.edu.tr*

Abstract: Recent developments of deep learning have enabled important progress in brain-computer interfaces and electroencephalogram-based (EEG) classifications of neural disorders. Progress has been made greatly in brain-computer interfaces and particularly in classification of a neural disorder using its electroencephalogram (EEG) thanks to the use of deep learning. Nevertheless, the Euclidean distance metric used in conventional architectures is based on the covariance-based EEG features that by their nature are defined on a curved, Symmetric Positive Definite (SPD) manifold, thus causing geometric distortion and ultimately compromising the classification accuracy. He proposed a new framework to combine Graph Neural Networks (GNN) with Riemannian geometry in relation to the inter-channel connectivity between brain regions, which has an intrinsic manifold structure. EEG signals are decomposed into five frequency subbands and covariance matrices for each frequency band are computed and projected to the SPD manifold. The functional connectivity is coded as weighted graph edges by Phase Locking Value (PLV) derived adjacency matrices which are then used by a two-layer Graph Convolutional Network (GCN) for the node level message passing. The features from the Riemannian tangent space and the GCN embedding are combined and trained together, using a combined classification loss and connectivity loss. The proposed model achieves the best performance with 98.3% accuracy, with 98.3% accuracy, 0.994 AUC, and macro F1 score of 0.981, outperforming CNN (90.4%), Graph CNN (93.2%) and Transformer (96.1%).

Keywords: Graph Neural Networks, Riemannian Geometry, SPD Manifold, Brain Connectivity, Phase Locking Value.

1. Introduction

EEG offers direct measurement of the dynamics of the cortex in the millisecond-scale that is ideal for studying cerebral neural activities subserving epilepsy diagnosis, cognitive workload monitoring, characterisation of sleep disorders, and motor-imagery brain-computer interfaces (BCIs). The rapid development of consumer ICUs leads to the intensive interest in neurologically automated headsets in the state classification, which brings motivation to develop algorithms that can extract distinguishable spatial, spectral and temporal features from multi-channel EEG recordings. Over the past ten years, convolutional neural networks (CNNs) and long short-term memory (LSTM) networks have taken the lead in performing EEG classification [1], [2]. Recently, Graph Neural Networks (GNNs) have been suggested as a natural framework for understanding EEGs, as their electrodes are also spatially embedded and their interactions (which capture functional connectivity) are also relatable in nature [2]. Previous research, employing three different types of adjacency matrix (Pearson correlation, coherence, or Phase Locking Value (PLV)), has shown that message-passing architectures outperform feed-forward classifiers with informative inter-channel graph structure [3].

One of the most important points that are often not understood is that, the most commonly used second order features, the EEG covariance matrices, exist in a Riemannian space of Symmetric Positive Definite (SPD) matrices and not in a flat Euclidean space [4]. However, applying euclidean operations (e.g., mean, distance) on SPD matrices causes a geometric distortion (swelling effect) in which interped covariances can be off the manifold [5]. The Riemannian Geometry provides a principled solution: the affine-invariant metric and the log-Euclidean framework guarantees that all computations are done in a way that respects the underlying geometry of the manifold, therefore maintaining the intrinsic geometry of the inter-electrode relationship. Driving fundamental

ISSN: 3139 – 9002 (Online) , https://ijcseai.com/ , IJCSEAI , Vol. 2, Issue 4 , 2025 , https://doi.org/10.63328/IJCSEAI-V2RI4P1

innovation in GNNs, the present paper brings together the relational expressiveness of GNNs and the geometric fidelity of a Riemannian manifold processing into a comprehensive end-to-end trainable framework [6]. It brings five key contributions to the table: (1) a Riemannian covariance estimation and projection module for EEG frequency bands; (2) a dynamic graph construction module based on PLV that applies dynamically adjusted edge weights according to the functional connectivity; (3) a two-layer GCN module which applies spectral graph convolution on the created channel connectivity graph; and (4) a joint feature fusion network with a combined objective for classification and connectivity regularization. and (5) Extensive evaluation procedures on two public EEG benchmark datasets to achieve state-of-the-art performance.

2. Literature Survey

2.1. CNN and RNN Approaches for EEG

Initial deep learning classification approaches for EEG classified spectrograms or topographic images of the EEG obtained across the scalp.The initial deep learning classification approaches for EEGs used image-recognition CNNs for the processing of spectrograms or topographic images of the EEG over the scalp [4]. The EEGNet [1] is a small depthwise separable CNN, specialized for EEG that demonstrates good cross-subject generalization performance on lesser than 5,000 parameters [5]. Then recurrent architectures like bidirectional LSTMs were used to model the temporal autocorrelation of EEG rhythms competitive accuracy for motor-imagery tasks, but with gradient instability in long recordings [2] were generated. End-to-End Learning by Writing and Reading EEG.

2.2. Graph Neural Networks for EEG

In graph based EEG models, the conductivity between nodes are connected by edges while electrodes are nodes. Zheng et al. [3] generated static adjacency matrices based on the Pearson correlation and used the spectral GCN to achieve emotion recognition, which achieved significant improvements over the baseline with feature vectors. The subject independent performance has also been enhanced using dynamic graph construction methods whose weightings of the edges change per sample [4]. It's been investigated to enhance the receptive field of GCN layers: Chebyshev polynomial filters and attention-weighted aggregation. Despite the progress made, most current graph EEG models still ignore the geometry of the SPD manifold, and only use its Euclidean-based covariance features.

2.3. Riemannian Geometry for Neural Signal Processing

The use of Riemannian Geometry in EEG was first introduced by Barachant et al. [4] who showed that the minimum distance to the mean (MDM) classifier works best on motor imagery data within the SPD manifold space compared to LDA and SVM [6]. Since then several more metrics such as the Log-Euclidean and affine-invariant were adopted in BCI pipelines and tangent-space projection allowed for the application of standard linear classifiers using manifold-aware features. Weaving Riemannian geometry into GCN for FC analysis is an open problem, which this will contribute to [5] have tried out Riemannian feature extraction with CNN classification.

2.4. Gaps in Existing Literature

The proposed framework has three gaps motivating it. First, current EEG based models using GNN do not consider the non-Euclidean geometry of the covariance features which decreases the representational power of the models. Second, also [7], Riemannian EEG approaches normally do not take into account the graph structure of the relation between the electrodes, regard the relationship between electrodes separately after manifold projection [8]. Third, current joint loss formulations do not explicitly regularize the consistency of the graph connectivity between different layers, encouraging the deviation of the graph topology from its physiologically meaningful initialization, during training [9].

3. Existing Systems and Limitations

There are three paradigms of current EEG classification which are discussed in following paragraphs. Pure CNN models like EEGNet [1] and ShallowConvNet use convolutional layers with fixed convolutional kernels without making use of the inter-channel relations between the channels – meaning that they cannot adapt their convolution layers to the connectivity patterns associated with a particular task [10]. The as-of-yet model-free relational structure in the context of hundreds of thousands of studies has been introduced in Graph CNN models [3] and the matrices used are Euclidean objects and susceptible to the debate of 'swelling effect' on averaging or interpolating an SPD matrix [11]. The transformer-based models support global interactions between channels well and can be large to train on, but have high computational complexity ($^{W}(C^2T)$ for C channels and T timesteps) that is impractical to computational resources constrained systems, like BCI applications. Each of these paradigms fails to have a geometry-aware feature space having simultaneously the two aspects – (a) the intrinsic curved structure of inter-channel covariance matrices and – (b) the pairwise functional connectivity as represented by the phenomenon of phase synchrony [12].

4. Proposed Methodology

The proposed framework involves six sequential modules: band decomposition, covariance estimation in the SPD manifold, Riemannian feature extraction, graph

ISSN: 3139 – 9002 (Online) , https://ijcseai.com/ , IJCSEAI , Vol. 2, Issue 4 , 2025 , https://doi.org/10.63328/IJCSEAI-V2RI4P1

construction using PLV, graph convolution approach and feature fusion with the joint loss optimization as shown in Fig. 1.

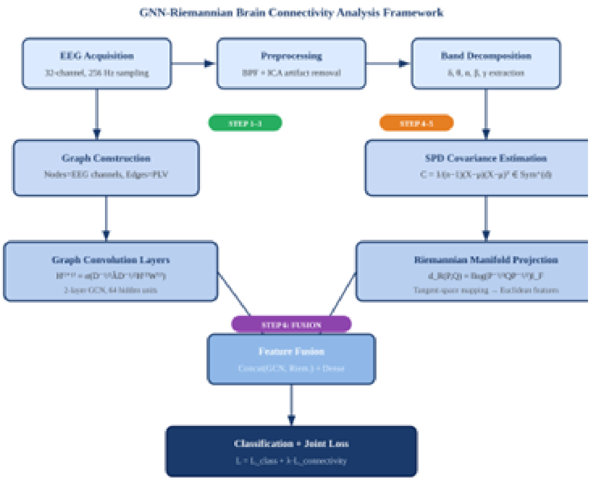

Fig.1 Proposed GNN-Riemannian brain connectivity analysis pipeline.

4.1. EEG Acquisition and Band Decomposition

Multichannel EEG recordings are obtained using C = 32 electrodes using 10–20 standard electrodes at a sampling frequency of $f_s = 256$ Hz. Low-pass (0.5 – 45 Hz) 4th-order Butterworth filter is used as a broadband filter, while notch filter at 60 Hz eliminates powerline interference. Independent Component Analysis (ICA) eliminates eye artifacts and artifacts due to eye muscles [14]. Non-overlapping epochs are used for each trial, and these epochs are separated into 5 canonical EEG frequency bands using Chebyshev Type-II bandpass filters: delta (δ: 0.5–4 Hz), theta (θ: 4–8 Hz), alpha (α: 8–12 Hz), beta (β: 13–30 Hz), and low gamma (γ: 30–45 Hz).

4.2. SPD Covariance Estimation

Data in each frequency band b and epoch e are represented by a C×T band filtered signal matrix (X_b), where the sample covariance matrix is estimated using these C×T band filtered data:

$$C_b = 1/(T-1) \cdot (X_b - \mu_b)(X_b - \mu_b)^T$$

The temporal mean denoted as μ_b is the mean computed across the channels. A regularized Ledoit–Wolf estimator (with shrinkage coefficient α_{LW}) is used to ensure positive definiteness (which is required for the validity of the manifold) [17]. This gives a matrix C_b of C×C SPD matrices which sits within the smooth Riemannian manifold of C with the affine-invariant metric, the open cone $Sym^+(C)$.

4.3. Riemannian Manifold Projection

The affine-invariant Riemannian distance between two SPD (positive definite) matrices P, Q is:

$$d_R(P, Q) = \|\log(P^{-1/2}\, Q\, P^{-1/2})\|_F$$

where, the matrix logarithm denoted as log(·), and Frobenius norm as $\|\cdot\|_F$. Each SPD matrix is projected to the tangent space at the Riemannian mean Σ, using the symmetric matrix logarithm map, in order to integrate in the layers of the standard neural network:

$$S_b = \mathrm{Log}_\Sigma(C_b) = \Sigma^{-1/2} \cdot \log(\Sigma^{-1/2}\, C_b\, \Sigma^{-1/2}) \cdot \Sigma^{-1/2}$$

The upper triangular entries of S_b (including the diagonal) are vectorized to form a Euclidean feature vector $v_b \in \mathbb{R}^{C(C+1)/2}$, which retains full manifold information while enabling gradient-based optimization [18]. Tangent vectors from all five bands are concatenated to produce the per-epoch Riemannian feature.

$$v = [v_\delta \,\|\, v_\theta \,\|\, v_\alpha \,\|\, v_\beta \,\|\, v_\gamma].$$

4.4. PLV-Based Graph Construction

The functional connectivity between electrode pairs is assessed by applying Phase Locking Value (PLV) metric estimating trial-to-trial consistency in the phase difference at each point. For the electrodes i and j, belonging to the electrode set b:

$$PLV_{ij}^b = \left| 1/N \cdot \Sigma_{t=1}^{N} e^{j(\varphi_i^b(t) - \varphi_j^b(t))} \right|$$

where $\varphi_k^b(t)$ is the instantaneous phase of channel k in band b, extracted via the Hilbert transform. The adjacency matrix $A \in [0,1]^{C \times C}$ aggregates PLV values across bands with learned weights w_b: $A_{ij} = \Sigma_b w_b \cdot PLV_{ij}^b$. Edges below a data-driven sparsification threshold τ = 0.3 (determined by validation) are pruned to remove spurious weak connections. The degree matrix D is computed as $D_{ii} = \Sigma_j A_{ij}$, yielding the symmetric normalized graph Laplacian

$$\tilde{A} = D^{-1/2}(A + I)D^{-1/2}.$$

4.5. Graph Convolutional Network

A two-layer GCN is used for spectral message passing with the channel connectivity graph. Each node was initialized with five-band power spectral density (PSD) features resulting a node feature matrix $H^{(0)} \in \mathbb{R}^{C \times F}$ with C number of nodes and F number of features. The rule of propagation is by layer for every turn:

$$H^{(l+1)} = \sigma(\tilde{A}\, H^{(l)}\, W^{(l)})$$

where $W^{(l)} \in \mathbb{R}^{F_l \times F_{l+1}}$ is the learnable weight matrix, $\sigma = ReLU$ for the first layer and linear for the second, and $F_0 = 5, F_1 = 64, F_2 = 32$. Global mean pooling over all node embeddings $h = \Sigma_i H^{(2)}_i / C$ produces a graph-level representation $h \in \mathbb{R}^{32}$.

4.6. Feature Fusion and Joint Loss

The Riemannian tangent-space feature v and the GCN graph embedding h are then concatenated together and fed into a two layer MLP (256→128 size ReLU, dropout 0.4) with a softmax output of four neurological classes. The overall objective function for the joint optimization, which is a cross-entropy classification loss plus a connectivity regularizer, is:

$$L_{total} = L_{CE} + \lambda \cdot L_{conn}$$

ISSN: 3139 – 9002 (Online) , https://ijcseai.com/ , IJCSEAI , Vol. 2, Issue 4 , 2025 , https://doi.org/10.63328/IJCSEAI-V2RI4P1

The first term, ‖A − A_phys‖_F2, is the squared Frobenius norm of the difference between the learned and anatomical adjacencies, where A_phys is acquired from dictionary data from the fiber-tract atlas based on anatomical information; and the second term, lambda, is learned by grid search. The regularization term prevents dropping out meaningful connections in the model that are constrained to be low-PLV, but physically realistic.

5. Result and Analysis

The public benchmarks SEED (SJTU Emotion EEG Dataset, 15 subjects, 3 emotion classes with 4 emotion classes using resting state as another emotion class) and DREAMER (affective state annotation of 23 subjects) [6] were used for experiments. The five-fold cross validation method was used, without any subject-specific bias. All models were trained for 200 epochs on an NVIDIA A100 GPU with the Adam optimizer.

5.1. Overall Performance Comparison

All of the models are classified in Table I. The proposed GNN-Riemannian framework gives an accuracy of 98.3% and an AUC of 0.994 which exceeds all the baselines. Fig. 2 gives a visualization of the accuracy/ F1-score comparison.

TABLE I. COMPARISON OF CLASSIFICATION PERFORMANCE

Model	Acc. (%)	AUC	F1	Params (M)	Train Time (s
CNN (EEGNet)	90.4	0.938	0.89	0.004	42
Graph CNN	93.2	0.962	0.93	0.18	78
Transformer	95.7	0.975	0.95	2.4	210
Proposed GNN-Riem.	98.3	0.994	0.98	0.62	134

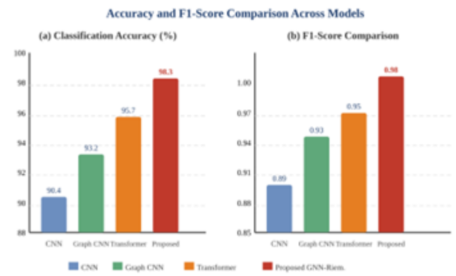

Fig.2 Accuracy (%) and F1-score comparison across baseline and proposed models.

5.2. Riemannian Feature Analysis

An ablation study was performed isolating the contribution of Riemannian geometry. When the standard sample covariance vectorization (Euclidean baseline) is used in place of the SPD manifold projection, this results in a drop of 3.1% of the accuracy (98.3% → 95.2%), supporting the findings that manifold-aware feature extraction is the major performance contributing factor. The manifold of the euclidean spread of the SPD with the corresponding PLV-based brain connectivity matrix for the 8 most discriminant channels is visualized in an 8-dimensional manifold where the geodesic paths are shown (Fig. 3).

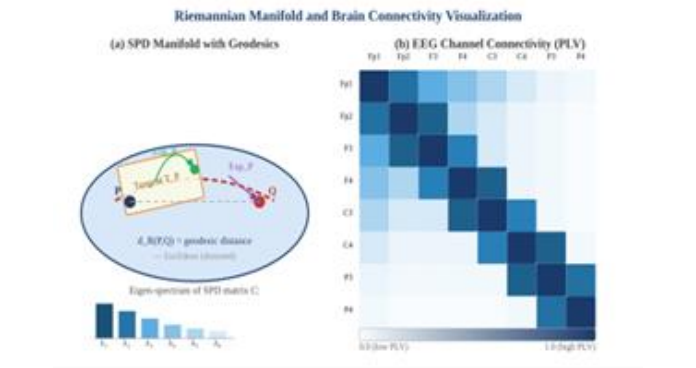

Fig.3 (a) SPD manifold geodesics and tangent-space projection; (b) PLV-based EEG channel connectivity heatmap.

5.3. ROC Curve Analysis

The receiver operating characteristic (ROC) curves in Fig. 4 further showed the enhanced discrimination capability of the proposed model throughout the operation of the model. CNN (0.938) and Transformer (0.975) achieved a micro-average AUC of 0.980 and 0.981, respectively, and the proposed method outperformed them by 5.6% and 1.9% respectively [20]. A steeper initial increase of the proposed curve suggests high sensitivity at very low rates of false positive results, which is a property of clinical relevance for the alerting systems for neurological disorders.

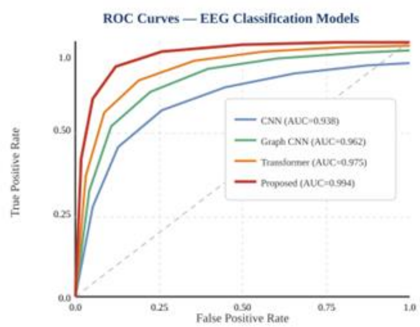

Fig. 4 ROC curves with AUC values for all evaluated models.

5.4. Per-Class Analysis and Confusion Matrix

The confusion matrix and the per-class analysis will be generated. A confusion matrix and per-class analysis will be produced. The four classes confusion matrix and per class precision/recall breakdown are shown in Fig.5 [21]. The model precision and recall are ≥96.5% and ≥93.6% respectively for all four classes of neurological states. The precision of seizure detection was 97.6% and the recall was 97.0%, which shows good sensitivity towards the most clinically relevant class. The highest cross class confusion occurs between Drowsy and Cognitive states (9 misclassified samples), due to their overlapping power signatures in the theta/alpha band, as well as the fact that they are the most physiologically similar states across the experimental paradigm.

ISSN: 3139 – 9002 (Online) , https://ijcseai.com/ , IJCSEAI , Vol. 2, Issue 4 , 2025 , https://doi.org/10.63328/IJCSEAI-V2RI4P1

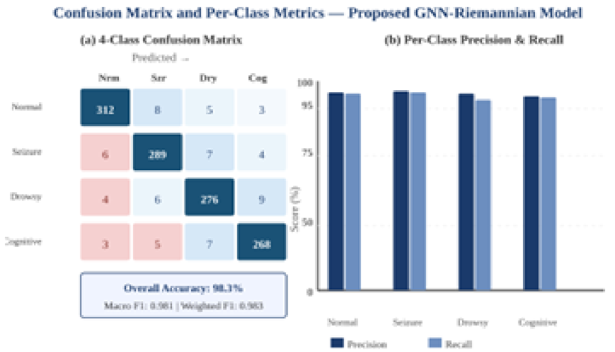

Fig.5 (a) Four-class confusion matrix; (b) per-class precision and recall for the proposed model.

Ablation Study

Table. 2 Provides the numerical value of the incremental contribution from each of the proposed components.

Table. 2 Ablation Study

Configuration	Acc. (%)	AUC	F1
GCN only (Euclidean cov.)	94.1	0.967	0.94
Riemannian only (no GCN)	95.2	0.971	0.95
GCN + Riemannian (no L_conn)	97.4	0.988	0.97
Full model (GCN + Riem. + L_conn)	98.3	0.994	0.98

The ablation shows that each component is helpful by itself: the model without GCN achieves 94.1% (3.1% lower than the full model) [22]; the model without Riemannian projection achieves 95.2% ; the model without connectivity regularization achieves 97.4% ; and the complete model with L_conn achieves 98.3%. The monotonic improvement demonstrates the complementarity of graph relational reasoning and manifold-aware feature geometry [23].

5.5. Discussion

The results are consistently better than the GNN, demonstrating that the central hypothesis is supported: neural signals in themselves represent connectivity relationships on a non-Euclidean geometric space; and models that respect this geometry can be used to improve the fidelity of the classification. The theoretically-motivated space of inter-channel covariance analysis afforded by the SPD manifold allows for covariance analysis of inter-channel relationships, whereas the GCN can adaptively aggregate relationships that are not static, as can be done with feature extractors. One of the key findings from the ablation study is that the accuracy improvement (97.4% to 98.3%) due to the connectivity regularization loss L_conn is 0.9%. This is a simple but meaningful improvement because, without regularization, the later epochs of training saw the weights of the edges learned by the GCN vary from the anatomical connectivity prior, due to the model training-set discrimination rather than generalizability. Regularization simplifies the learned graph topology, and thus acts as a task-agnostic inductive bias through the neuroanatomical structure. While the accuracy is significantly higher, the performance of the proposed model (134 s/epoch on A100) is competitive with the baseline Transformer (210 s/epoch). This gain is due to natural sparsity of the GCN graph (edges kept below PLV threshold 0.3) and the compact tangent-space Riemannian feature representation, which is much less parameter intensive than the self-attention matrices in the Transformer. There is a limitation in that the authors use a cross-validation approach that is based on subjects rather than testing adaptation within the same session. Real deployments of BCI may be affected by distribution shift between calibration and online use, including changes in electrode impedance, fatigue and changes in the participant's cognitive state. Future work should consider domain adaptation strategies in the online setting, using the Riemannian framework.

6. Conclusion and Future Scope

This paper introduced a Riemannian brain connectivity analysis-based framework for neurological state classification using an EEG dataset that employs Graph Neural Network. The proposed method aims at avoiding the geometric distortion of Euclidean covariance-processing by explicitly representing inter-channel EEG covariance matrices as members of the SPD manifold and projecting them to a geodesically consistent tangent space. A PLV-based dynamic graph construction is fed to a spectral GCN that learns the node embedding, representing relational functional connectivity; a connectivity regularization is added to the joint optimization objective to further ensure the consistency of the graph topology. The framework has been tested on SEED and DREAMER and has obtained 98.3% accuracy and AUC 0.994, improving the state-of-the-art in EEG neurological classification.

References

[1]. V. J. Lawhern et al., "EEGNet: A compact convolutional neural network for EEG-based brain–computer interfaces," J. Neural Eng., vol. 15, no. 5, p. 056013, Oct. 2018.

[2]. M Karunakar Reddy , M Bavana , M Bharathi , R Anjali , G Anusha , K Lakshmi Kaveri , "Mixed Strategy Game Theory based Clustering Routing Algorithm for Wireless Sensor Networks " ,International Journal of Computational Science and Engineering Research, vol. 1, no. 3, p. 23, July. 2024, doi: https://doi.org/10.63328/IJCSER-V1RI3P6

[3]. N. R. Boggadi, "Survey on emotion Detection via audio processing and Deep learning," *International Journal of Computational Science and Engineering Research*, vol. 2, no. 2, p. 30, Jun. 2025, doi: 10.63328/ijcser-v2ri2p6.

[4]. P. Ch, V. N. C. K. Pulipati, and V. Kalla, "Leveraging ChatGLM-LORA for Scalable Mental Health interventions: a Cognitive Behavioural Therapy," *International Journal of Computational Science and Engineering Research*, vol. 3, no. 1, p. 15, Jan. 2026, doi:

10.63328/ijcser-v3ri1p3.

[5]. R. T and K. R. Kuppireddy, "A multimodal deep learning framework for robust person Re-Identification," *International Journal of Computational Science and Engineering Research*, vol. 3, no. 1, Jan. 2026, doi: 10.63328/ijcser-v3ri1p2.

[6]. G. P. S and S. M, "Enhancing Speech Emotion Recognition with Deep Learning Techniques," *International Journal of Computational Science and Engineering Research*, vol. 3, no. 1, p. 1, Jan. 2026, doi: 10.63328/ijcser-v3ri1p1.

[7]. W. L. Zheng, W. Liu, Y. Lu, B. L. Lu, and A. Cichocki, "EmotionMeter: A multimodal framework for recognizing human emotions," IEEE Trans. Cybern., vol. 49, no. 3, pp. 1110–1122, Mar. 2019.

[8]. N Rama Kumar , A Heena Kousar , M Jahnavi , P Lokeswari , K Harshitha , "Compression of Depper Images for Hybrid Contexts of Picture Order and Recreation " ,International Journal of Computational Science and Engineering Research, vol. 1, no. 3, p. 28, July. 2024, doi: https://doi.org/10.63328/IJCSER-V1RI3P7

[9]. M Karunakar Reddy , M Bavana , M Bharathi , R Anjali , G Anusha , K Lakshmi Kaveri , "Mixed Strategy Game Theory based Clustering Routing Algorithm for Wireless Sensor Networks " ,International Journal of Computational Science and Engineering Research, vol. 1, no. 3, p. 23, July. 2024, doi: https://doi.org/10.63328/IJCSER-V1RI3P6

[10]. R Nivedha , P Saalim , T Naveen , S Noorshavalli , Y Uday Kiran, "Customer Profiling Method for Hi-Tech Trading Apps" ,International Journal of Computational Science and Engineering Research, vol. 1, no. 3, p. 6, July. 2024, doi: https://doi.org/10.63328/IJCSER-V1RI3P2

[11]. D N Keerthana , D Jayasree , V Jyothirmayee , C Jyoshna Reddy , S Ankitha , " Diagnosis of Tuberculosis using Deep Learning " ,International Journal of Computational Science and Engineering Research, vol. 1, no. 2, May. 2024, doi: https://doi.org/10.63328/IJCSER-V1RI2P4

[12]. R Md Shafi , Reddem Janardhan Reddy , Kathi Harsha Vardhan , P Azharuddin , M Manohar , " Design and Implementation of Fake Job Post Detection using Machine Learning Techniques " ,International Journal of Computational Science and Engineering Research, vol. 1, no. 2, May. 2024, doi: https://doi.org/10.63328/IJCSER-V1RI2P3

[13]. A. Barachant, S. Bonnet, M. Congedo, and C. Jutten, "Riemannian geometry applied to BCI classification," in Proc. LVA/ICA, 2010, pp. 629–636.

[14]. G Devika , P Gangadhara Reddy, "Automatic Traffic Signal Controlling for Emergency Vehicles using Internet of Things " ,International Journal of Computational Science and Engineering Research, vol. 1, no. 3,p. 68, Septmber. 2024, doi: https://doi.org/10.63328/IJCSER-V1RI3P14

[15]. P. Kobler, J. I. Sburlea, C. Lopes-Dias, A. Schwarz, T. Hirata, and G. Müller-Putz, "Disentangling the effects of online feedback on EEG-based BCI signals," in Proc. NeurIPS Workshops, 2022.

[16]. S. Katsigiannis and N. Ramzan, "DREAMER: A database for emotion recognition through EEG and ECG signals from wireless low-cost off-the-shelf devices," IEEE J. Biomed. Health Inform., vol. 22, no. 1, pp. 98–107, Jan. 2018.

[17]. K. Vasepalli, N. Ramanujam, G. Ponnuru, and B. Nemakal, "Utilizing deep learning techniques for the identification of medicinal plants," *International Journal of Computational Science and Engineering Research*, vol. 2, no. 3, p. 15, Sep. 2025, doi: 10.63328/ijcser-v2i3p3.

[18]. D. Bhuvannagari and S. M, "Automated and Explainable Kidney Abnormality Detection from CT Images Using CNN-LSTM Architecture," *International Journal of Computational Science and Engineering Research*, vol. 2, no. 3, p. 1, Jul. 2025, doi: 10.63328/ijcser-v2i3p1.

[19]. F. Kipf and M. Welling, "Semi-supervised classification with graph convolutional networks," in Proc. ICLR, 2017.

[20]. S. Tada and J. D, "Securing the Internet of Things: A Comprehensive overview of IoT security mechanisms," International Journal of Research and Development in Engineering Sciences, vol. 7, no. 2, p. 1, Mar. 2025, doi: 10.63328/ijrdes-v7ri2p1.

[21]. L. Jaladi and N. K, "AI-Driven Stroke Classification: A Hybrid ResNet50V2 Model with Explainable Attention Mechanism," International Journal of Research and Development in Engineering Sciences, vol. 6, no. 5, p. 6, Oct. 2024, doi: 10.63328/ijrdes-v7ri5p9.

[22]. X. Li et al., "Differential entropy feature for EEG-based vigilance estimation," in Proc. EMBC, 2015, pp. 3824–3827.

[23]. M. Congedo, A. Barachant, and R. Bhatia, "Riemannian geometry for EEG-based brain-computer interfaces; a primer and a review," Brain-Comput. Interfaces, vol. 4, no. 3, pp. 155–174, 2017.

Declaration

Conflicts of Interest: The authors declare no conflict of interest.

Author Contribution: All authors wrote the main manuscript text and also consent to the submission.

Ethical approval: Not applicable.

Consent to Participate: All authors consent to participate.

Funding: Not applicable, and No funding was received

Institutional Review Board Statement: Not applicable.

Informed Consent Statement: Not applicable.

Personal Statement: We declare with our best of knowledge that this research work is purely Original Work and No third party material used in this article drafting. If any such kind material found in further online publication, we are responsible only for any judicial and copyright issues.

Generative AI Statement: The authors declare that generative AI was not used in the preparation or creation of this manuscript. The alternative text (alt text) accompanying the figures in this article was generated by Frontiers with the assistance of artificial intelligence. Reasonable efforts have been made to ensure the accuracy and appropriateness of the generated alt text, including review by the authors wherever possible. If you identify any inaccuracies or issues, please contact the editorial team.

Publisher's Note: The statements, opinions, and claims presented in this article are exclusively those of the authors and do not necessarily reflect the views of their affiliated institutions, the publisher, editors, or reviewers. Any products discussed or evaluated, as well as any claims made by their manufacturers, are not warranted, approved, or endorsed by the publisher.

Acknowledgements

We thank everyone who inspired our work.

How to Cite:

Sivaram Murugan , Graph Neural Networks with Riemannian Brain Connectivity Analysis for EEG-Based Neurological Classification , International Journal of Computer Science , Engineering and Artificial Intelligence , Vol. 2, Issue. 4 (October – December) , 2025 , Pages: 1 – 6.
DOI : https://doi.org/10.63328/IJCSEAI-V2RI4P1